The Astrophysical Journal, 689:231–241, 2008 December 10
© 2008. The American Astronomical Society. All rights reserved. Printed in U.S.A.

THE KINEMATICS OF KEPLER'S SUPERNOVA REMNANT AS REVEALED BY *CHANDRA*

Jacco Vink[1]

Received 2008 March 18; accepted 2008 August 8

ABSTRACT

I have determined the expansion of the supernova remnant of SN 1604 (Kepler's supernova) based on archival *Chandra* ACIS-S observations made in 2000 and 2006. The measurements were done in several distinct energy bands, and were made for the remnant as a whole, and for six individual sectors. The average expansion parameter indicates that the remnant expands on average as $r \propto t^{0.5}$, but there are significant differences in different parts of the remnant: the bright northwestern part expands as $r \propto t^{0.35}$, whereas the rest of the remnant's expansion shows an expansion $r \propto t^{0.6}$. The latter is consistent with an explosion in which the outer part of the ejecta has a negative power law slope for density ($\rho \propto v^{-n}$) of $n = 7$, or with an exponential density profile [$\rho \propto \exp(-v/v_e)$]. The expansion parameter in the southern region, in conjunction with the shock radius, indicates a rather low value ($<5 \times 10^{50}$ erg) for the explosion energy of SN 1604 for a distance of 4 kpc. A higher explosion energy is consistent with the results if the distance is larger. The filament in the eastern part of the remnant, which is dominated by X-ray synchrotron radiation, seems to mark a region with a fast shock speed $r \propto t^{0.7}$, corresponding to a shock velocity of $v = 4200$ km s^{-1}, for a distance to SN 1604 of 4 kpc. This is consistent with the idea that X-ray synchrotron emission requires shock velocities in excess of $\sim$2000 km s^{-1}. The X-ray–based expansion measurements reported are consistent with results based on optical and radio measurements but disagree with previous X-ray measurements based on *ROSAT* and *Einstein* observations.

Subject headings: ISM: individual (Kepler's supernova) — shock waves — supernova remnants — X-rays: ISM

Online material: color figures

1. INTRODUCTION

Among the more than 250 known Galactic supernova remnants, the remnants of the historical supernovae hold a special place (Stephenson & Green 2002). This has partially to do with the fascination for historical events that caught the imagination of astronomers in ancient China, the Middle East, and in renaissance Europe. But also more scientific reasons make the study of historical supernova remnants worthwhile: we know the exact age of the objects. Moreover, the historical supernova remnants are among the youngest supernova remnants, which means that their X-ray emission is largely dominated by shock-heated ejecta rather than shocked interstellar matter. Historical remnants are therefore prone to offer new insights into the supernova explosion properties.

The youngest historical supernova remnant (SNR) is SN 1604 (Stephenson & Green 2002), also known as Kepler's SNR (Kepler for short).[2] The supernova was first sighted on the evening of 1604 October 9, low above the horizon. It owes its early discovery probably to the much anticipated simultaneous conjunction of Jupiter, Saturn, and Mars. Johannes Kepler lived in Prague at that time and was hindered by bad weather. However, from the first reports on he took a keen interest in the new star, and after the weather improved, he started his own observations. The results of his observations and his correspondence with other observers led to his book on the supernova, *De Stella Nova*, which was published in 1606.

The SNR of SN 1604 has been a puzzling object for some time (Blair 2005). Both the historical light curve of the supernova (Baade 1943) and its relatively high Galactic latitude ($l = 4.5^\circ$, $b = 6.4^\circ$) suggest that Kepler is the result of a Type Ia supernova. However, optical observations of the remnant reveal the presence of copious amounts of nitrogen, in particular in the northwest. Nitrogen is an element associated with stellar winds rather than Type Ia supernovae. This prompted Bandiera (1987) to suggest that the progenitor was a massive, runaway star, thus explaining both the origin of nitrogen and the high Galactic latitude of the supernova. Nevertheless, the X-ray spectrum of Kepler indicates a large abundance of iron, which points to a Type Ia supernova (Kinugasa & Tsunemi 1999; Cassam-Chenaï et al. 2004). A recent deep *Chandra* observation revealed no evidence for a neutron star (Reynolds et al. 2007), which would be expected if SN 1604 was a core-collapse supernova. Having considered all evidence, Reynolds et al. (2007) conclude that Kepler is the remnant of a Type Ia supernova from a relatively massive progenitor star, attributing the nitrogen to stellar wind loss from either the white dwarf progenitor or the companion star.

The situation concerning the kinematics of Kepler is equally confusing. Dickel et al. (1988) studied the expansion of Kepler in the radio, based on VLA 6 cm and 20 cm data covering a time span of 4 yr. They found expansion rates indicating significant deceleration with, on average, an expansion rate consistent with a radial expansion law $r \propto t^{0.5}$, and in the northern part even as low as $r \propto t^{0.35}$. Optical expansion measurements, based on ground-based and *Hubble Space Telescope* imaging of the bright Hα filaments in the northwest covering a time span of 16.33 yr, showed proper motions of 1.3″–1.6″ (Sankrit et al. 2005). This corresponds to an expansion law following $r \propto t^{0.35}$, consistent with the radio measurements. However, X-ray expansion measurements, based on *Einstein* and *ROSAT* observations with the high-resolution imagers on board these two satellites, indicated nearly free expansion: $r \propto t^{0.93}$ (Hughes 1999). Note that of all wavelength regimes the X-ray emission is most closely associated with the dynamics of the remnant, since the shock-heated plasma has most of its emission in X-rays, and best compares with hydrodynamic simulations. The optical emission is confined to a region close to the shock front, whereas the kinematics as derived from the radio

[1] Astronomical Institute, Utrecht University, P.O. Box 80000, 3508TA Utrecht, Netherlands; j.vink@astro.uu.nl.

[2] Cas A is a younger remnant, but not strictly a historical remnant, because the supernova was likely not observed (Stephenson & Green 2002).

emission should be related to the X-ray–emitting plasma, but the mismatch between radio and X-ray expansion measurements for Kepler, but also Cas A (Vink et al. 1998; Koralesky et al. 1998; Delaney & Rudnick 2003) and Tycho's SNR (Hughes 2000), complicates the interpretation.

Resolving the discrepancy between radio and X-ray expansion measurements and obtaining the overall kinematics of Kepler's SNR is important for several reasons: First of all the distance to the SNR is poorly known. One way to estimate the distance is to measure both the proper motion and the shock velocity. The latter can be done independent of the proper motion by measuring the broad Hα emission line, which is the result of charge transfer from neutral hydrogen entering the shock to shock-heated protons. The broadening of the line therefore is a measure of the proton temperature, which is linked to the shock velocity. For Kepler this method yields a shock velocity of 1550–2000 km s^{-1} (Fesen et al. 1989; Blair et al. 1991), implying a distance of $3.9^{+1.4}_{-0.9}$ kpc (Sankrit et al. 2005). This is slightly lower than, but consistent with, the most recent measurement based on H I absorption features, 4.8 ± 1.4 kpc (Reynoso & Goss 1999).

Another issue is the dynamical state of the SNR. As long as the mass of the ejecta dominates over the mass of shock-heated circumstellar material the remnant is little decelerated and said to be in the free expansion phase with $R \propto t$ (see, however, Truelove & McKee 1999). Once the energy in the shock-heated circumstellar medium dominates the total energy, the SNR is said to have entered the Sedov-Taylor stage of its evolution with $R \propto t^{0.4}$ for a uniform-density medium. If SN 1604 is a Type Ia supernova, one expects it to have a relatively low ejecta mass of 1.4 $M_{\odot}$. A high expansion rate, as found in X-rays, is therefore puzzling.

Finally, in recent years it has been found that all young SNRs have thin filaments at the shock front, whose emission is dominated by synchrotron radiation (e.g., Vink & Laming 2003; Bamba et al. 2005; Völk et al. 2005). The widths of these filaments can be used to infer magnetic fields (e.g., Vink & Laming 2003; Bamba et al. 2005; Völk et al. 2005; Warren et al. 2005), which turn out to be relatively high. This is therefore evidence for cosmic-ray–driven magnetic field amplification (Bell & Lucek 2001; Bell 2004). However, it is not quite clear how the magnetic field scales with density and shock velocity; it could be either $B^2 \propto \rho v^2$ (Völk et al. 2005) or $B^2 \propto \rho v^3$ (Bell 2004; Vink 2006). The range in densities among the SNRs is quite large (a factor of 100 from SN 1006 to Cas A), so the dependency of B^2 on ρ can be determined reasonably well. However, X-ray synchrotron filaments only arise for high shock velocities $v \gtrsim 2000$ km s^{-1} (Aharonian & Atoyan 1999), and since all known SNRs have $v \lesssim 6000$ km s^{-1}, the dynamic range in velocity is not very high, as compared to the dynamic range in densities. Moreover, the uncertainties in the measured velocities are quite high. A more accurate assessment of the shock velocities in those regions where X-ray synchrotron filaments have been found (Reynolds et al. 2007) is therefore valuable. In addition, the cutoff photon energy of X-ray synchrotron radiation depends not only on v_s but also on the cosmic-ray diffusion parameter (Aharonian & Atoyan 1999):

$$E_{\rm cutoff} = 0.5\eta^{-1}\left(\frac{v_s}{2000\ {\rm km\ s^{-1}}}\right)^2\ {\rm keV}, \qquad (1)$$

with η a parameter that expresses the diffusion coefficient as a factor with respect to the Bohm diffusion coefficient. For Bohm diffusion, $\eta = 1$, the magnetic field is highly turbulent, resulting in fast cosmic-ray acceleration (see Malkov & Drury 2001 for a review). Apparently, $\eta \approx 1$ for young SNRs (Vink 2004, 2006; Stage et al. 2006). Accurate shock velocity measurements are therefore important for estimating the diffusion constant and the related turbulence of the magnetic field. Here I present expansion measurements based on archival *Chandra* data obtained in 2000 and 2006.

TABLE 1
Observations

Observation	Start Date	MJD	Exposure (ks)
116.....	2000 Jun 30 12:04:56	51,725.5034	49.45
6714.....	2006 Apr 27 23:13:49	53,852.97	159.84
6715.....	2006 Aug 03 16:52:09	53,950.70	161.17
6716.....	2006 May 05 19:18:18	53,860.80	160.05
6717.....	2006 Jul 13 19:04:25	53,929.79	108.18
6718.....	2006 Jul 21 14:55:14	53,937.62	109.18
7366.....	2006 Jul 16 05:24:07	53,932.23	52.12

2. DATA AND METHOD

2.1. *Observations*

Chandra observed Kepler several times, the first time in 2000 June as part of the Guaranteed Time Observation program. The most recent observation was made in 2006 as part of the Large Program (Reynolds et al. 2007). All observations were made with the ACIS-S array, with the SNR being projected on the ACIS-S3 chip.

Since proper-motion measurements are more reliable for longer time spans, I limited the analysis to the 2000 and 2006 observations, ignoring an additional observation made in 2004. The 2006 observation was split in several pointings, which we list in Table 1. Weighting the modified Julian dates (MJDs) of the 2006 with the exposure times, I obtain an average MJD for the 2006 observations of 53912.13. I therefore find an average time span between the 2006 and the 2000 *Chandra* observations of $\Delta t = 5.985$ yr.

For the analysis I used the standard processed ("evt2") event files obtained from the *Chandra* data archive. All event files were processed by the *Chandra* data center in 2007.

2.2. *Method*

The expansion measurements were made using the same method and updated C^{++} code employed for the SNR Cas A using *Einstein* and *ROSAT* observations (Vink et al. 1998). The results for Cas A were later confirmed by measurements based on *Chandra* observations (Delaney & Rudnick 2003). The method is similar to what has been used to measure the previous X-ray expansion of Kepler (Hughes 1999) and Tycho's SNR (Hughes 2000). One aspect not explored by these studies is the dependence of the expansion on the energy band, which was not possible due to lack of energy resolution of *Einstein* and *ROSAT*.

For the current analysis I extracted images in several energy bands using custom-made software, which, as described below, allows one to center the image on a given sky coordinate and correct for boresight errors. I chose energy bands based on the spectroscopic features of the X-ray spectrum (see Fig. 1): 0.5–0.7 keV (covering the O VII/O VIII line emission), 0.7–1.0 keV (Fe XVII–Fe XXI L-shell emission), 1.0–1.5 keV (Fe XXII–Fe XXIV L-shell emission, perhaps blended with Ne IX/X and Mg XI/XII emission), 1.7–1.9 keV (Si XIII K-shell emission), 2.0–4.0 keV (covering K-shell emission from Si, S, Ar, and Ca), and 4.0–6.0 keV, which is dominated by continuum emission (a combination of thermal bremsstrahlung and synchrotron radiation).

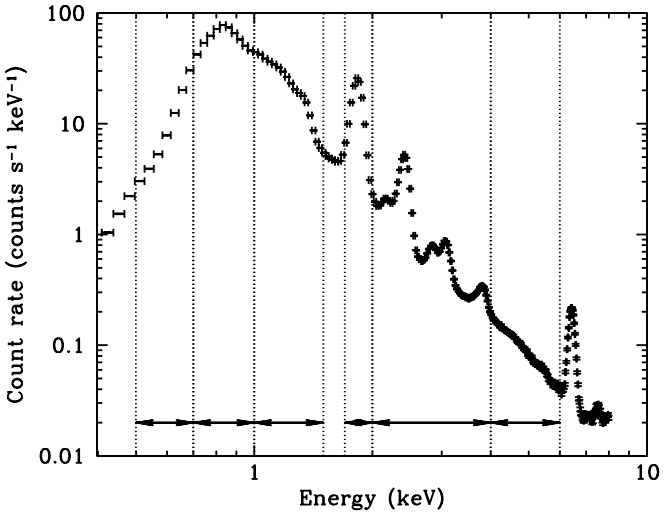

FIG. 1.—*Chandra* ACIS-S X-ray spectrum of the entire remnant, based on all 2006 observations (Reynolds et al. 2007). The arrows and dotted lines mark the energy bands used to measure the expansion. [*See the electronic edition of the Journal for a color version of this figure.*]

The expansion factor, f, was measured by regridding the images from the 2006 observations, which are statistically superior, using a simple expansion law:

$$x_2 = \mathrm{round}[x_0 + f(x_1 - x_0) + \Delta x], \qquad (2)$$
$$y_2 = \mathrm{round}[y_0 + f(y_1 - y_0) + \Delta y],$$

with (x_1, y_1) being the original pixel coordinates, (x_2, y_2) the new pixel coordinates (rounded to the nearest integers), and $(\Delta x, \Delta y)$, free parameters that are fitted to correct for pointing errors between the observations. The absolute roll angle accuracy is very high, $\sim 25''$, and therefore roll angle errors do not contribute to registration errors.[3] Note that pointing errors are indistinguishable from errors in the expansion center. For the expansion center (x_0, y_0) I adopted an estimate of the geometrical center of the remnant based on the X-ray image: $\alpha_{\mathrm{J2000}} = 17^{\mathrm{h}}30^{\mathrm{m}}41.25^{\mathrm{s}}$ and $\delta_{\mathrm{J2000}} = -21^{\circ}29'32.95''$.

For obtaining the best-fit expansion rates, maximum likelihood statistic for Poisson distributions was used (Cash 1979), which minimizes

$$C = -2 \ln P = -2\Sigma_{i,j}(n_{i,j} \ln m_{i,j} - m_{i,j} - \ln n_{i,j}!), \qquad (3)$$

with $n_{i,j}$ being the counts in pixel (i,j) of the ObsID 116 (2000) image, and $m_{i,j}$ being the predicted counts based on the 2006 image, which has been regridded (eq. [3]) and renormalized such that $\Sigma_{i,j} n_{i,j} = \Sigma_{i,j} m_{i,j}$. The statistical fluctuations are dominated by the observation in 2000 June, with its 49 ks exposure. I can therefore treat the combined 2006 observations with an exposure of 750 ks as a model. Note that the last term in equation (3) can be ignored for fitting purposes because it depends only on $n_{i,j}$, which does not change from one set of fit parameters to the other, as long as the numbers of bins remain unchanged. The error in the fit parameters can be estimated using the fact that $\Delta C = C - C_{\min}$ is similar to $\Delta\chi^2$ (Cash 1979). The fitting procedure itself is done by scanning the relevant parameter range, iteratively switching between the various parameters, and with each iteration decreasing the step size.

The code has the option to fit only certain regions of the image, using a combination of image masks and region files. For the overall fits a mask was used, based on the broadband image, blocking out all pixels falling below a certain threshold level. I fine-tuned this mask, such that the SNR image, smoothed with $\sigma = 2$ pixels plus a border of 2 additional pixels, falls within the mask.

A problem with equation (3) is that one can only sum over model pixels $m_{i,j}$ that are not zero. Regridding the model image makes it the case that in low-emissivity regions a model pixel may accidentally be set to zero for one set of parameters, in which case it is ignored, whereas for other values of the fit parameters it is nonzero. Hence, the number of pixels over which the statistic is derived is not constant. This problem does not occur for Kepler's SNR for energy bands with sufficient statistics, such as those covering the bright Fe L emission, but it is important for the continuum image. In order to overcome this problem the model image (based on the 2006 observations) was smoothed with a Gaussian with $\sigma = 1$ pixel, ensuring that the number of pixels over which the statistic is derived remained constant. I checked for the images with the best statistics whether smoothing had any effect on the expansion measurements, but within the statistical error the small-scale smoothing did not affect the measured expansion rates. For that reason I adopted Gaussian smoothing to all 2006 images, in order to have one consistent way of measuring for all energy bands.

The *Chandra* ACIS chips have a pixel resolution of $0.492''$, slightly undersampling the telescope point-spread function. Because of boresight effects, absolute coordinates are accurate up to $\sim 0.4''$. This means that by adding all the 2006 observations one may introduce a slight blurring by approximately 1 pixel. In order to start from the best possible images I used the same code as for expansion measurements reported below, but fixing $f = 1$, and using a broadband (0.3–7 keV) image. All fits were made with respect to the ObsID 6714 image. Having fitted $(\Delta x, \Delta y)$ for each individual observation, I made the final extraction of the images with corrections for the individual boresights, after which images in the same energy band were added together. The average boresight was 0.4 pixels in both coordinates, with rms errors of 0.2 pixels.

Throughout this paper I use three different ways of characterizing the expansion of Kepler's SNR: (1) the expansion rate defined as $R = (1 - f)/\Delta t$, with $\Delta t = 5.985$ yr; (2) the expansion time $\tau_{\mathrm{exp}} = 1/R$, which is perhaps the most intuitive number, as it gives the age of the remnant in case one assumes free expansion; (3) the expansion parameter $\beta = \tau_{\mathrm{SN\,1604}}/\tau_{\mathrm{exp}}$, the ratio of the true age of Kepler's SNR over the expansion time.

From a hydrodynamical point of view β is the most important parameter. In general, the shock radius, r_s, of SNRs in distinct different phases evolves with time τ as (Truelove & McKee 1999)

$$r_s = K\tau^{\beta}, \qquad (4)$$

with K a constant. This gives for the shock velocity

$$v_s = \beta \frac{r_s}{\tau}; \qquad (5)$$

this shows that

$$\beta = v_s \frac{\tau}{r_s} = \frac{\dot{\theta} d}{\theta d}\tau = \frac{(1 - f)}{\Delta t}\tau = R\tau, \qquad (6)$$

with d the distance and θ the angular radius.

3. RESULTS

3.1. *The Average Expansion*

The simplest approach to measuring the expansion of Kepler is to fit for each energy band the expansion factor and boresight/expansion center offsets $(\Delta x, \Delta y)$. Of course, both

[3] See http://cxc.harvard.edu/cal/ASPECT/roll_accuracy.html and T. Aldcroft (2008, private communication).

TABLE 2
EXPANSION RATES

Energy Band	R (% yr^{-1})	Δx (pixels)	Δy (pixels)	R ($\Delta x/\Delta y$ fixed) (% yr^{-1})
0.5–0.7 keV	0.084 ± 0.004	−0.58	−0.38	0.084 ± 0.004
0.7–1.0 keV	0.108 ± 0.002	−0.58	−0.38	0.106 ± 0.002
1.0–1.5 keV	0.115 ± 0.002	−0.67	−0.45	0.108 ± 0.002
1.7–2.0 keV	0.119 ± 0.003	−0.57	−0.38	0.117 ± 0.003
2.0–4.0 keV	0.131 ± 0.004	−0.74	−0.47	0.129 ± 0.004
4.0–6.0 keV	0.158 ± 0.006	−0.70	−0.61	0.155 ± 0.007
Mean (±rms)	0.119 ± 0.025	−0.64	−0.44	0.116 ± 0.024
β	0.48 ± 0.10	...	...	0.47 ± 0.10
$\tau_{\rm exp}$	840 ± 181	...	...	859 ± 185

the expansion center and boresight errors should not depend on the energy band. So a second iteration involves fixating $(\Delta x, \Delta y)$ and then measuring the expansion of the remnant.

However, this is still not ideal; Kepler's SNR is bright in the northwest, so expansion measurements of the whole remnant are skewed toward the northwest. Moreover, since a next step involves measuring the expansion in different regions, errors in $(\Delta x, \Delta y)$ result in errors in the expansion rate, with opposite signs for opposite sides of the SNR.

I therefore adopted a different method: I first divided the SNR into four sectors of each 90°. Instead of fitting the four sectors individually, I paired them in north-south and east-west pairs. For the north-south pair I fixated Δy and for the east-west pair Δx. This ensures that there is no interference between proper-motion and boresight corrections, since $(\Delta x, \Delta y)$ are measured perpendicular to the proper motions. This procedure was repeated twice in an iterative way for the four energy bands with sufficient counts (the oxygen, two Fe L bands, and Si band). The best-fit values are $(\Delta x, \Delta y) = (-0.48 \pm 0.01, -0.35 \pm 0.04)$, which were then used for all subsequent expansion measurements.

Table 2 lists the expansion rates for the individual energy bands both with $(\Delta x, \Delta y)$ as free parameters, and fixed to the aforementioned best-fit values. Figure 2 shows the expansion parameter β for the individual energy bands. Comparing the expansion rate measurements for fixed and fitted $\Delta x/\Delta y$ shows that the measured expansion rates are, within the statistical error, identical. The likelihood ratios (ΔC) for the individual fits show smooth curves as a function of expansion rate, indicating that the minimum value for the statistic is well defined, with no subminima (Fig. 3).

There is a clear tendency for the expansion parameter to increase with the photon energy, ranging from $\beta = 0.34 \pm 0.02$ for the oxygen band to $\beta = 0.62 \pm 0.03$ for the continuum band. Note that these values are significantly lower than the expansion parameters reported by Hughes (1999).

Figure 4 shows the effect of taking the average expansion into account for the 1.0–1.5 keV band, by showing the difference between the 2000 and 2006 images. The difference image shows some image artifacts across the northern shell. These are caused by streaks in the 2000 June images. The streaks are not immediately obvious in the images themselves, but the difference image emphasizes them, in particular when the expansion has been corrected for. Similar artifacts showed up in measuring the expansion of Cas A with *Chandra* (Delaney & Rudnick 2003). From the residuals after expansion correction, I estimate that the brightness errors across the streaks are typically ∼10%, except near the

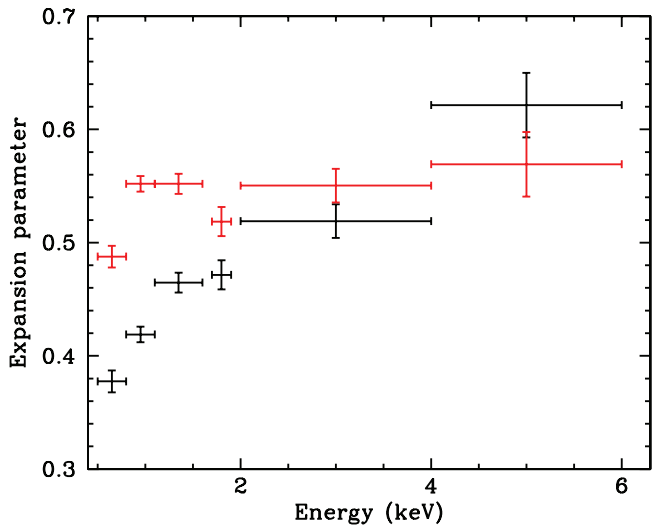

FIG. 2.—Expansion parameter as function of energy. The overall expansion rates, based on fitting the expansion for the whole remnant, are indicated in black. The errors correspond to 90% confidence ranges. Due to the brightness of the northwestern region, the expansion rates are biased toward the expansion in the Northwest. The expansion rate averaged over all six sectors is displayed in red, with errors corresponding to the standard deviation.

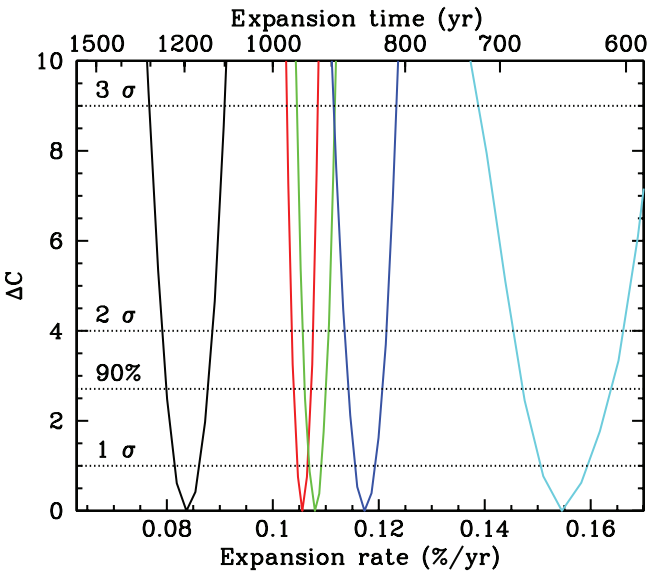

FIG. 3.—Confidence ranges for the expansion rates for the remnant as a whole, based on the log likelihood ratio, ΔC, with respect to the best fit (Cash 1979). From left to right the curves correspond to the energy bands 0.5–0.7 keV (O VII/O VIII line emission), 0.7–1.0 keV (Fe L line emission), 1.0–1.5 keV (Fe L line emission), 1.7–1.9 keV (Si XIII line emission), and 4.0–6.0 keV (continuum emission).

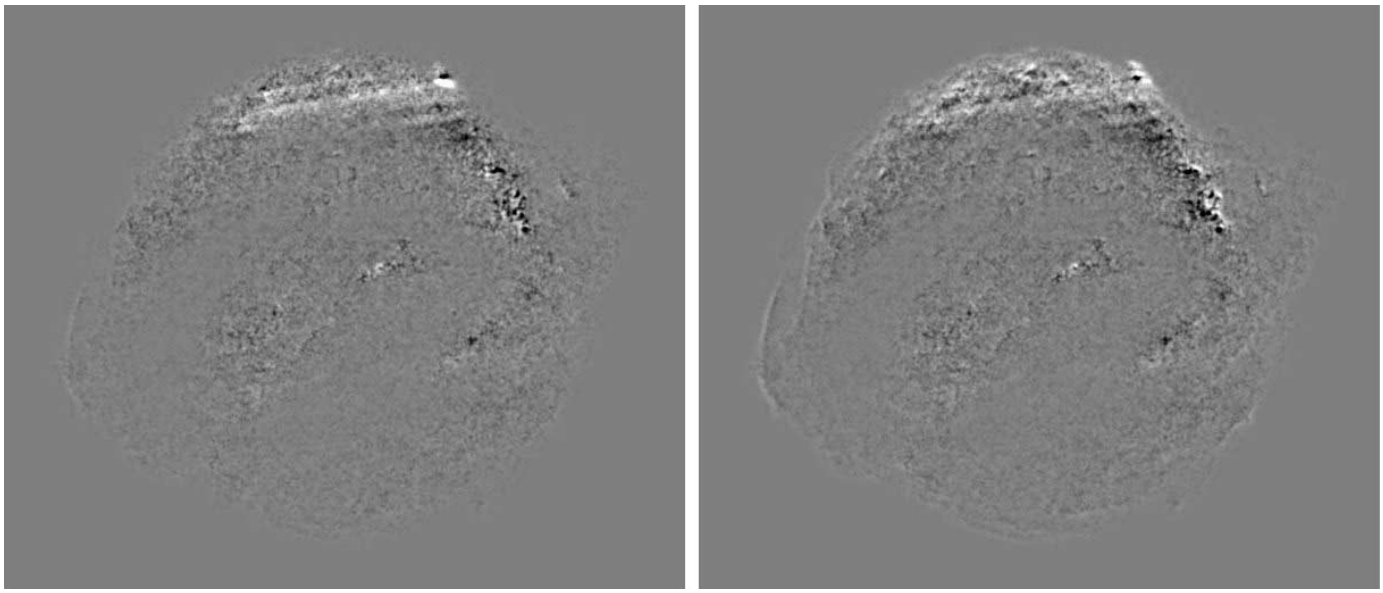

FIG. 4.—Difference between the 2000 and 2006 1.0–1.5 keV image. A small Gaussian smoothing has been applied to the images ($\sigma = 1$ pixel). The image on the right has only been corrected for the boresight error. The 2006 image on the left has also been corrected for the average expansion. Note that the left image still shows some expansion of the filament in the east, and overcorrects some of the expansion in the west (see § 3.2). Also note the image artifacts in the north, which are more visible in the left-hand image, because there the expansion has been taken out, leaving the artifacts as one of the dominant sources of differences between the two images.

bright knot, where the brightness error peaks to ~30%. Here it is not quite clear whether the large deviations are caused by the streaks or by the knot itself. I come back to the streaks below.

3.2. *The Expansion as a Function of Azimuth*

Given the strong asymmetry of Kepler's SNR it is quite natural to expect that the expansion will also be asymmetric, as indeed was found by Dickel et al. (1988) in the radio. I investigated this by dividing the remnant in six sectors, each spanning 60° in azimuthal angle (Fig. 5). In order to measure only proper motions around the shell of the remnant, the central region was ignored, which features a barlike structure of unknown origin (Fig. 5). For the measurements of the expansion per sector, the same expansion center and boresight corrections were applied for each sector as for the mean expansion measurements reported in § 3.1.

In total 36 expansion rates were measured, covering six sectors and six X-ray bands. The expansion rates as a function of azimuthal angle are listed in Table 3, whereas the expansion parameters and expansion times are displayed in Figure 6. The expansion rates averaged over all sectors show less variation as a function of energy than the mean expansion rates based on the whole remnant. An important difference is that the averaged rates give equal weight to all sectors of the remnant, whereas the mean expansion rate is biased toward the brighter northwest of the remnant (Fig. 2).

Table 3 and Figure 6 show that the expansion in the north-northwestern sectors is considerably slower than in the other parts of the remnant: for the northwestern sector the expansion parameter ranges between $\beta = 0.3$ and 0.4, corresponding to $\tau_{\rm exp} = 1000$–1500 yr. For the southern and eastern sectors this is $\beta = 0.55$–0.68, corresponding to $\tau_{\rm exp} = 590$–730 yr. Figure 6 also suggests that the variation in the average expansion as a function of energy (Fig. 6) can be mostly attributed to the northwestern region.

As shown in Figure 4 there are streaks in the 2000 June images, which happen to be confined to the northern sector. The expansion measurements in this sector give an expansion parameter similar to that of the neighboring northwestern sector. Given the presence of artifacts in this region one should treat this expansion measurement with more caution than those of the other five sectors. In order to have a quantitative estimate of the streaks on the expansion measurements of the northern region, I also measured the expansion rate after blocking out most of the pixels affected by the streaks, thus removing about half of the northern sector. Using this smaller region resulted in a higher expansion rate, corresponding to $\beta = 0.5$, except for the 4–6 keV band, which remained at $\beta = 0.3$. Either this difference could be attributed to the removal of the streaks, i.e., the value listed in Table 2 for the northwestern region could be affected by systematic errors of order 30%, or it could be that the regions blocked out have slower expansion rates. The latter option is quite well possible, since the streaks affect mostly the western part of the northern sector, i.e., the region closest to the more slowly expanding northwestern sector. In that case the different rates of expansion are due to a gradient across this sector, which is quite plausible. Given the uncertainty, I will not explicitly discuss the northern region, but instead concentrate on the contrast between the slow expansion in the northwest and the rest of the remnant.

3.3. *The X-Ray Synchrotron Filament in the Southeast*

As mentioned in § 1, the shock velocity near X-ray synchrotron filaments is of considerable interest for understanding both magnetic field amplification (Bell 2004; Völk et al. 2005; Vink 2006) and the magnetic field turbulence. Like Cas A and Tycho, Kepler's SNR shows continuum emission around the whole periphery of the remnant, some of which is probably X-ray synchrotron emission (e.g., Cassam-Chenaï et al. 2004). However, in the northwest the continuum emission is more diffuse and associated with regions of the most intense line radiation. It is therefore quite likely that most, if not all, of the continuum emission from this region is thermal bremsstrahlung. The most unambiguous X-ray synchrotron–emitting filament is the arclike filament in the east. As shown by Cassam-Chenaï et al. (2004) and Reynolds et al. (2007) the spectrum of this filament is completely dominated by continuum emission. The width of this filament was used by Völk et al. (2005) to infer a magnetic field of 250 μG (see also Bamba et al. 2005). The 2006 observations also show that the filament is narrow, 2.5″. However, note that the estimate of the magnetic

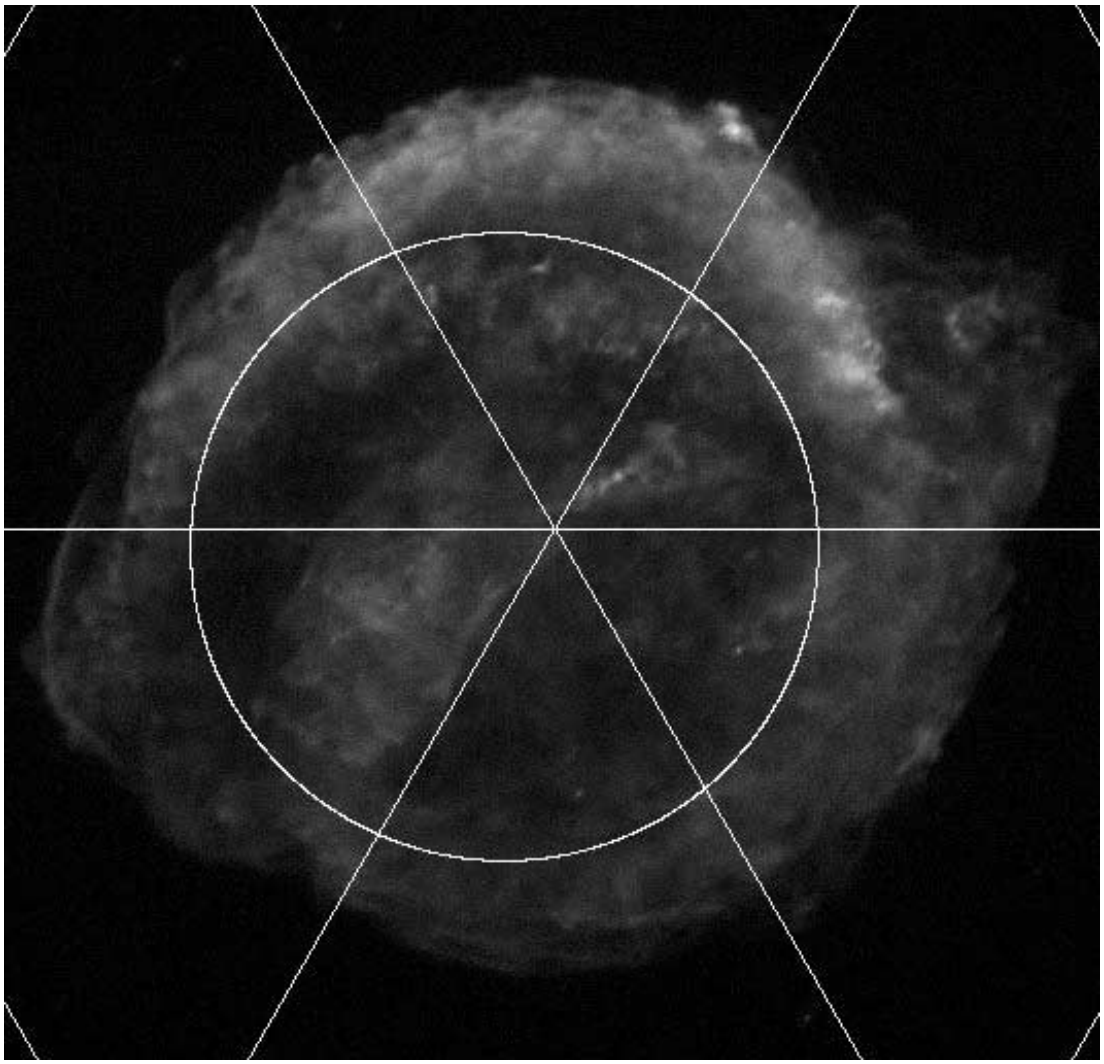

FIG. 5.—Color image combining the 1.0–1.5 keV (*red*), 1.7–2.0 keV (*green*), and 4–6 keV (*blue*) with overlaid the sectors used for measuring the expansion as a function of azimuth. The circle indicates the region not considered for the expansion measurements. [*See the electronic edition of the Journal for a color version of this figure.*]

field by Völk et al. (2005) assumes spherical symmetry in order to estimate the true, deprojected, filament width. Taking the 2.5″ at face value results in a magnetic field of 85 μG using the formula in Vink et al. (2006). This should be taken as a conservative lower limit.

Since it is important to know under what conditions X-ray synchrotron emission occurs, I measured the expansion of the eastern filament separately. Figure 7 shows the exact region for the measurement. The spectrum from this filament shows hardly any line emission (Reynolds et al. 2007), so I measured the expansion using a 0.3–7 keV broadband image in order to improve the statistics of the measurements. The expansion rate that is found is $R = 0.176\% \pm 0.007\%$, corresponding to a relatively large expansion parameter of $\beta = 0.71 \pm 0.03$. The filament is located at an angular radius of 2.1′ from the center. Since X-ray synchrotron filaments trace the shock front, one can therefore translate the expansion parameter into a shock velocity of $v_s = (4200 \pm 170) d_4$ km s^{-1}, with d_4 the distance in units of 4 kpc. This is twice

TABLE 3
EXPANSION RATES PER SECTOR

	R (% yr^{-1})					
SECTOR	0.5–0.7 keV	0.7–1.0 keV	1.0–1.5 keV	1.7–1.9 keV	2.0–4.0 keV	4.0 –6.0 keV
0 (N)	0.074 ± 0.007	0.098 ± 0.002	0.096 ± 0.003	0.105 ± 0.005	0.108 ± 0.006	0.080 ± 0.015
60 (NE)	0.094 ± 0.011	0.133 ± 0.004	0.141 ± 0.005	0.134 ± 0.007	0.140 ± 0.010	0.171 ± 0.021
120 (SE)	0.168 ± 0.022	0.164 ± 0.010	0.174 ± 0.006	0.160 ± 0.011	0.173 ± 0.008	0.178 ± 0.014
180 (S)	0.155 ± 0.028	0.148 ± 0.012	0.164 ± 0.013	0.143 ± 0.014	0.154 ± 0.014	0.109 ± 0.016
240 (SW)	0.116 ± 0.018	0.160 ± 0.008	0.143 ± 0.009	0.139 ± 0.011	0.143 ± 0.013	0.173 ± 0.021
300 (NW)	0.068 ± 0.006	0.077 ± 0.003	0.081 ± 0.004	0.093 ± 0.007	0.103 ± 0.009	0.138 ± 0.021
Mean (±rms)	0.113 ± 0.042	0.130 ± 0.035	0.133 ± 0.037	0.129 ± 0.025	0.137 ± 0.027	0.142 ± 0.04

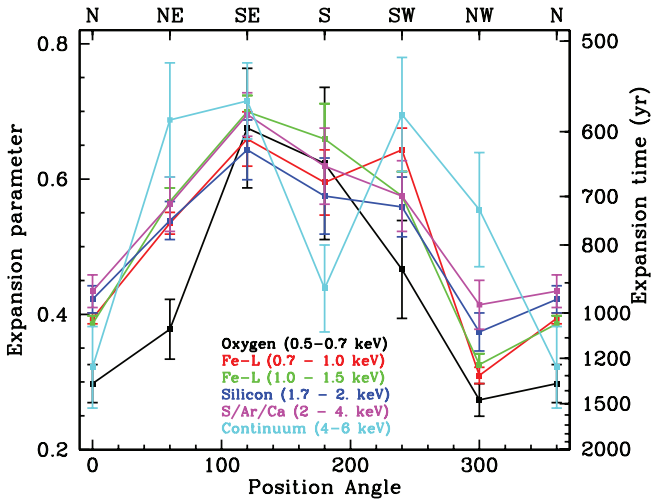

FIG. 6.— Expansion parameter of Kepler's SNR as a function of azimuthal angle. The angle is measured from the north in a counterclockwise direction. The different colors indicate expansions measured in different energy bands, using the same color coding as in Fig. 3. The data points have been cyclic, so the data points at 360° repeat those at 0°. The vertical axis on the right indicates the corresponding expansion time.

as fast as the shock velocities inferred from optical spectral and proper-motion studies in the northwestern region (Blair et al. 1991; Sankrit et al. 2005) but consistent with the value adopted by Völk et al. (2005).

Since the shape of the filament has a radius of curvature smaller than the radius of the remnant, one may wonder in what directions the filament is actually expanding: is the filament caused by a blowout, in which case one expects the expansion center to be closer to the approximate curvature center of the filament, or is the expansion center close to the geometrical center of the whole remnant? In order to get some handle on this, I also fitted the expansion, but leaving the center of expansion as free parameters. In that case, the best-fit center of expansion was more toward the west ($\alpha_{J2000} = 17^h30^m40.77^s$, $\delta_{J2000} = -21°29'29.49''$) than the adopted center, i.e., opposite of the nonthermal filament. This, and in addition blinking of the 2000 and 2006 images by eye, suggests that the curved structure is moving more or less as a coherent structure rather than expanding from a center close to the filament. This is reminiscent of the kinematics of a bow shock structure. The expansion parameter did not change substantially when the expansion center was treated as a free parameter: $\beta = 0.67 \pm 0.04$.

4. DISCUSSION

I have measured the expansion of Kepler's SNR using archival *Chandra* data from observations performed in 2000 and 2006. These new X-ray expansion measurements largely agree with expansion measurements based on radio (Dickel et al. 1988) and optical (Sankrit et al. 2005) measurements. Specifically, the results confirm that the average expansion parameter is $\beta \approx 0.5$. The expansion as a function of azimuthal angle shows a clear difference in expansion rate between the northwestern and other parts of the remnant, with the northwestern part having an expansion parameter $\beta \approx 0.3$–0.4, as also found in the radio (Dickel et al. 1988) and optical (Sankrit et al. 2005), and the other parts having $\beta \approx 0.6$, in agreement with the radio measurements.

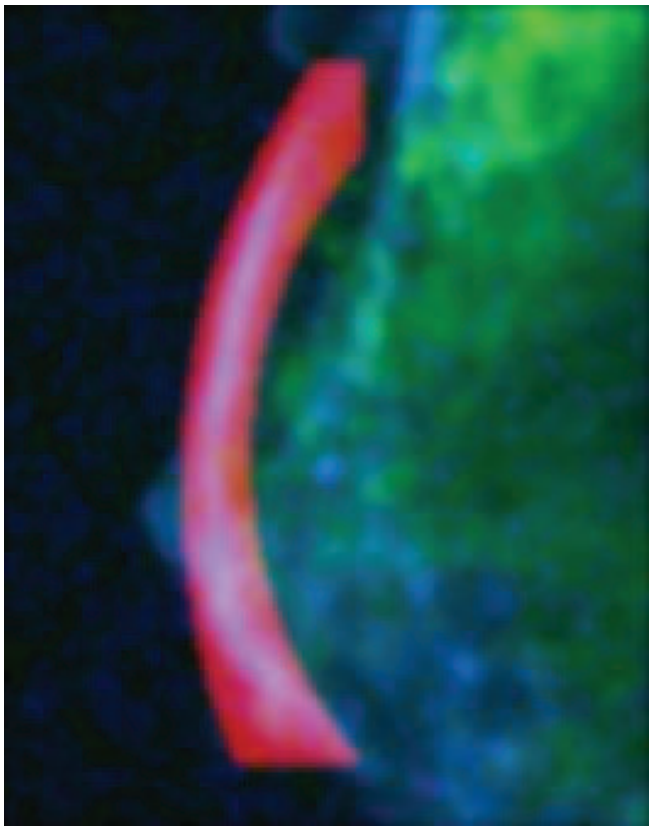

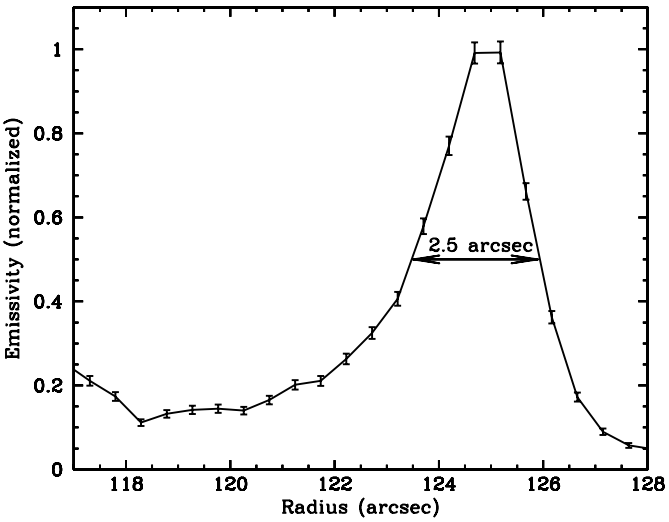

FIG. 7.—*Left:* Detail of the eastern part of Kepler's SNR, showing in red the mask used for determining the proper motion of the filament, in green the broadband image, and in blue a smoothed version of the 4–6 keV image. *Right:* Emissivity profile of the northern region of the filament, based on the 2006 *Chandra* observations in the 4–6 keV band.

The expansion measurements presented here are in disagreement with previous X-ray measurements, based on *ROSAT* and *Einstein* data (Hughes 1999), which suggested $\beta \approx 0.9$. In terms of resolution this new measurement should be better than the *ROSAT-Einstein* measurement, despite the long baseline of the latter, 17.5 yr. The resolution of the high-resolution imagers on board the *ROSAT* and *Einstein* satellites is about $4''$, amounting to $0.22''$ yr^{-1} for a baseline of 17.5 yr. The pixel resolution of the *Chandra* ACIS instrument is $0.43''$, so the resolution per unit time for the present study is about $0.07''$ yr^{-1}. It is difficult to assess what causes the discrepancy between the new result and the *ROSAT*/*Einstein* study, as the measurements by Hughes (1999) used a similar method as employed here and for the expansion of Cas A (Vink et al. 1998 also based on *Einstein* and *ROSAT* data).

4.1. *The Expansion Parameter in Theoretical Models*

Theoretical models of SNR evolution directly predict the expansion parameter, a dimensionless number (Chevalier 1982; Dwarkadas & Chevalier 1998; Truelove & McKee 1999). The best-known example is the evolution of the shock wave in the so-called Sedov-Taylor phase, which treats the supernova as a point explosion in a uniform-density medium. This gives $\beta = 0.4$. Chevalier (1982) analyzed the early evolution of a SNR, in the context of power-law ejecta density models, i.e., $\rho \propto v^{-n}$. This gives $\beta = (n-3)/n$ for an explosion in a uniform-density medium. For Type Ia supernovae it has been argued that $n = 7$, which should therefore result in $\beta = 0.57$ during the early phase of the SNR.

The expansion parameter in this case refers to both the contact discontinuity (separating shocked circumstellar medium [CSM] and shocked ejecta) and the forward shock. The plasma in the shell has a range of expansion parameters centered around $\beta = 0.57$, ranging from $\beta = 0.63$ near the reverse shock to $\beta = 0.43$ near the forward shock.

Dwarkadas & Chevalier (1998) studied the hydrodynamical evolution of Type Ia remnants numerically, using both power-law ejecta density profiles and an exponential ejecta density profile [$\rho \propto \exp(-v/v_e)$]. They explicitly provide the expansion parameter of the shock itself, which in the case of the exponential density profile ranges from $\beta = 0.8$ very early in the evolution to $\beta = 0.4$, although never reaching $\beta = 0.4$. The expansion parameter of the shocked plasma can be obtained from their Figure 3: at a late phase, around $t \approx 500 E_{51}^{-0.5} n_0^{-1/3}$ yr (n_0 being the preshocked number density and E_{51} the explosion energy in units of 10^{51} erg), for both types of density profiles $\beta \approx 0.5$–0.6 for the forward shock, but for the plasma the expansion parameter is almost uniformly $\beta \approx 0.38$. The lower expansion parameter for the plasma is not surprising, given that the plasma directly behind the shock moves with $v = 3v_s/4$ in the case of a monatomic gas with adiabatic index $\gamma = 5/3$. Therefore, in the late phase $\beta_{\rm shock} = 4\beta_{\rm plasma}/3$.

These studies are important for interpreting the measured expansion parameters of Kepler's SNR. First, it is good to be aware that the expansion parameters of the shock may be different from those of the plasma. In the late phase, the plasma expansion parameter is lower than that of the shock itself, whereas in the early phase of the evolution there is a range of values, but around the contact discontinuity the expansion parameter is similar to that of the shock. Therefore, during the early evolution the expansion parameter is expected to be close to the expansion parameter of the forward shock.

4.2. *Inferences on the Shock Velocities*

The question now arises, what do the X-ray expansion measurements really provide: the expansion parameter of the shock or that of the plasma behind it? The shock velocity is a pattern speed, and this is certainly part of what is measured. As Figure 4 shows, correcting for the mean expansion removes the strong fringes in the difference map, around the forward shock. On the other hand, the velocity of the plasma itself also may influence the best-fit expansion parameters. The measurements themselves are skewed toward the outer part of the shell, simply because the proper motions are larger there and more pixels are involved.

The models discussed above therefore suggest that the measured expansion parameter is a lower limit to the expansion parameter of the forward shock, later in the evolution of the SNR (i.e., $t' > 1$ in the notation of Dwarkadas & Chevalier 1998, their eq. [6]). In an earlier phase, for which the Chevalier (1982) models may be applicable, the measured expansion parameter may be a good representation of the expansion parameter of the forward shock.

The expansion measurements for most of the remnant, except for the northwestern part, give $\beta \approx 0.6$, which is consistent with the expansion parameter of $\beta = 0.57$ for both the contact discontinuity and the forward shock for the $n = 7$ model of Chevalier (1982), the preferred model for Type Ia supernovae. It is also in the approximate range for the forward shock expansion parameter for the exponential density profile model considered by Dwarkadas & Chevalier (1998) but only in the case in which the remnant is still in the early phase of its evolution, i.e., if the self-similar time variable is $t' \lesssim 1$.

Note that the theoretical values for the expansion parameter, whether for the shock or the plasma, are all lower than the expansion parameters obtained from the previous X-ray measurements based on *ROSAT* and *Einstein* observations (Hughes 1999), namely, $\beta = 0.93$. The Chevalier (1982) model for $n = 7$ gives for the plasma velocities a range of $\beta = 0.4$–0.6, whereas the exponential density profiles gives $\beta < 0.8$ after the first few decades in the life of the SNR (Dwarkadas & Chevalier 1998). In addition, the previous X-ray expansion measurements are inconsistent with the Fe K emission detected to come from reverse shocked material in Kepler's SNR, as discussed by Cassam-Chenaï et al. (2004); Fe K emission requires a well advanced reverse shock and high reverse shock speed, which is incompatible with free expansion.

The values for the expansion parameter in the southern and eastern sectors are consistent with the expansion parameter for the $n = 7$ model of Chevalier (1982), which applies to both the contact discontinuity and the forward shock. It seems, therefore, justified to translate the measured expansion parameter into a shock velocity, using that the average angular radius of Kepler is $r = 1.76'$. This gives $v_s = 3010(\beta/0.6) d_4$ km s^{-1}, with d_4 the distance in units of 4 kpc.

For the northwestern region shock velocities have been measured using the widths of Hα lines, which gives a direct measurement of the postshock proton temperature. These suggest shock velocities in this region of 1500–2800 km s^{-1} (Fesen et al. 1989; Blair et al. 1991), with the most likely value centered around 1660 km s^{-1} (Sankrit et al. 2005). The proper motions of the Hα-emitting shock regions are $0.088''$ yr^{-1} (Sankrit et al. 2005). This corresponds to an optical expansion parameter of $\beta = 0.33$. This value is consistent with the value reported here for the X-ray expansion parameter for the northwestern region, $\beta = 0.3$–0.4, and with the radio expansion parameter $\beta \approx 0.35$.

Finally, the highest expansion reported in this paper is for the X-ray synchrotron filament in the east ($\beta = 0.71$). The size of the X-ray synchrotron–emitting region is determined by the loss time of the highest energy electrons and their advection away from the shock front (Vink & Laming 2003; Vink 2006). As a result, the size of the X-ray–emitting region is expected to be fixed as long as the magnetic field and the shock speed are approximately

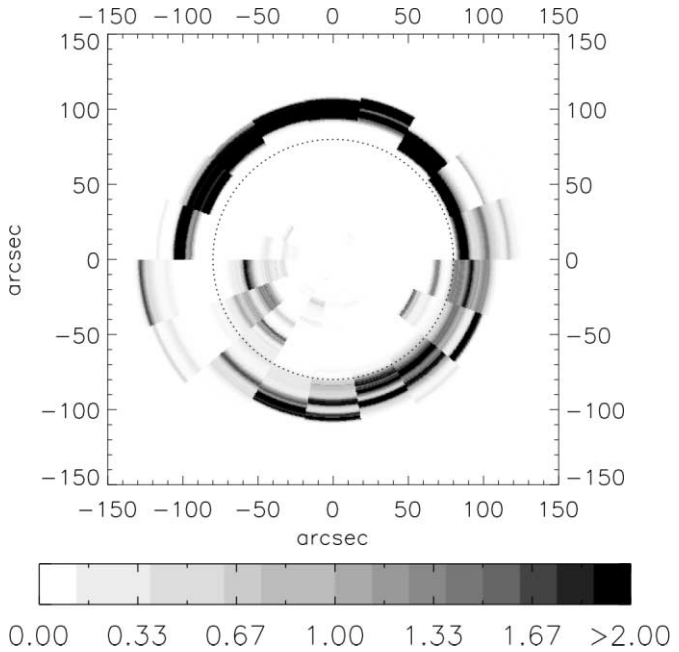

FIG. 8.—Deprojected 1–1.5 keV (Fe L) image of Kepler's supernova remnant, used to estimate the location of the reverse shock (indicated by the dotted line with a radius of 1.3′). The deprojection was made in 18 independent sectors, following the procedure described in Helder & Vink (2008). The brightness scale is in percentage per bin, scaled in such a way that the total adds up to 100% integrated flux in each sector. (Figure kindly provided by Eveline Helder.)

constant. The displacement of the filament therefore reflects the speed of the shock front, rather than the movement of the plasma. This suggests that the measured filament movement is a pattern movement, and directly reflects the movement of the shock front, implying $v_s = 4200 d_4$ km s^{-1}.

This relatively high shock velocity and the protrusion of the filament outside the general shock radius of Kepler's SNR make it quite likely that the filament marks a part of the shock that is expanding into a low-density region, as previously suggested by Cassam-Chenaï et al. (2004). Moreover, the high velocity and the low density both help to explain why in this region X-ray synchrotron emission dominates over thermal emission. The high velocity is consistent with the idea that only shocks with velocities $v_s \gtrsim 2000$ km s^{-1} give rise to detectable X-ray synchrotron radiation (Aharonian & Atoyan 1999; Vink et al. 2006; Helder & Vink 2008).

4.3. *The Expansion and the Energetics of SN 1604*

The regions of Kepler's SNR that are likely to be most revealing about the explosion parameters of SN 1604 are the southern/southwestern regions. In the northwestern region it is clear that the expansion parameter is too low to fit either the models of Chevalier (1982) and Dwarkadas & Chevalier (1998) or the Sedov evolution. In the east the radius of the remnant is not well determined, due to the protruding nonthermal filament. For the southwestern region the shock radius is 1.77′, corresponding to a physical radius of $r_s = 2.06 d_4$ pc. As an additional constraint we can use the radius of the reverse shock. From the 1–1.5 keV (Fe L) image the typical reverse shock radius is estimated to be $\sim$1.3′ (Fig. 8), corresponding to a reverse shock radius of $r_r \approx 1.6 d_4$ pc. Using these values, and the measured expansion parameters for the southern/southwestern regions ($\beta \approx 0.6$) in conjunction with the models of Truelove & McKee (1999) or Dwarkadas & Chevalier (1998), we can constrain the preshock density and explosion energy for Kepler's SNR.

Figure 9 shows the $n = 7$ Truelove & McKee (1999) model for two different choices of kinetic energy and circumstellar medium density, assuming a distance of 4 kpc. One choice is to assume that $n_{\rm H} = 1$ cm^{-3}, the other that the energy is the canonical explosion energy of $E_0 = 10^{51}$ erg ($\equiv$1 Bethe). In both cases it has been assumed that the ejecta mass is $M_{\rm ej} = 1.4\,M_\odot$, as is to be expected for a Type Ia supernova (Woosley et al. 2007; Mazzali et al. 2007 for recent discussions on this issue). It is clear that both in terms of the reverse shock position in Kepler's SNR and in terms of measured expansion parameters a lower kinetic energy is to be preferred.

Comparing the measured properties for the southern part of Kepler's SNR with the numerical models of Dwarkadas & Chevalier (1998) leads to a similar conclusion. The measured expansion parameters are consistent with a low value of the self-similar time coordinate in Dwarkadas & Chevalier (1998), i.e., $t' \lesssim 1$, with $\beta \approx 0.6$, corresponding to $t' \approx 0.6$. However, a conservative upper limit is $t' < 2$, corresponding to $\beta = 0.5$ for the shock itself. Translating the dimensionless time and the associated normalized shock radii ($0.85 \lesssim r' \lesssim 1.6$) into a physical age and shock radius using the conversion equations in Dwarkadas & Chevalier (1998) equations (4)–(6), one finds that $0.7 \lesssim n_{\rm H}/({\rm cm}^{-3}) \lesssim 5$ and $0.2 \lesssim E_0/(1\ {\rm B}) \lesssim 0.5$, with a preference for the lower values.

Thus, for both the Truelove & McKee (1999) and Dwarkadas & Chevalier (1998) models it appears that SN 1604 had a relatively low explosion energy. However, this also depends on the adopted distance of 4 kpc (Sankrit et al. 2005). For 5 kpc, close to the nominal distance estimate of Reynoso & Goss (1999), the allowed range of densities and energies is $0.4 \lesssim n_{\rm H}/({\rm cm}^{-3}) \lesssim 2.5$ and $0.3 \lesssim E_0/(1\ {\rm B}) \lesssim 0.9$, which is still rather low compared to the uniform kinetic energies of 1.2 ± 0.2 B inferred for observed Type Ia supernovae (Woosley et al. 2007). Moreover, the upper limit requires a relatively high density for a SNR located $470 d_4$ pc above the Galactic plane. Only for an adopted distance of 6 kpc is the angular radius of the forward and reverse shock of the SNR consistent with a kinetic energy of 10^{51} erg. The associated ISM density is then $n_{\rm H} = 0.5({\rm cm}^{-3})$. A distance considerably farther than 4 kpc seems therefore preferable, provided that SN 1604 was indeed a Type Ia supernova, and considering the evidence that most Type Ia supernovae have energies in excess of 10^{51} erg (Woosley et al. 2007).

A similar conclusion was recently obtained based on the nondetection of TeV emission from Kepler with the H.E.S.S. telescope (Aharonian et al. 2008). Note that the conclusion of Aharonian et al. (2008) depends on assumptions concerning the TeV luminosity of the remnant, which depends on the explosion energy and on the fraction of the energy that goes into accelerating cosmic rays.

4.4. *Estimates of the Swept-up Mass in the Northwest*

The northwestern region of Kepler's SNR has an expansion parameter even lower than the expansion parameter expected for the Sedov-Taylor phase. This is probably caused by a nonuniform density profile. The northwestern part of the remnant shows in the optical nitrogen-rich material, suggesting a shell ejected by the progenitor system. The fact that the expansion rate in the northwestern region seems to be a function of photon energy may be accounted for if the inner layer of shocked ejecta is hotter and if in this layer the expansion parameter is larger. The slowest expansion is measured for the oxygen band, and it has been suggested that most oxygen emission is from shocked circumstellar medium, rather than from the ejecta (Cassam-Chenaï et al. 2004). The trend with energy in this region could be an effect of a slow response of the inner layers to density enhancements closer to the shock. This

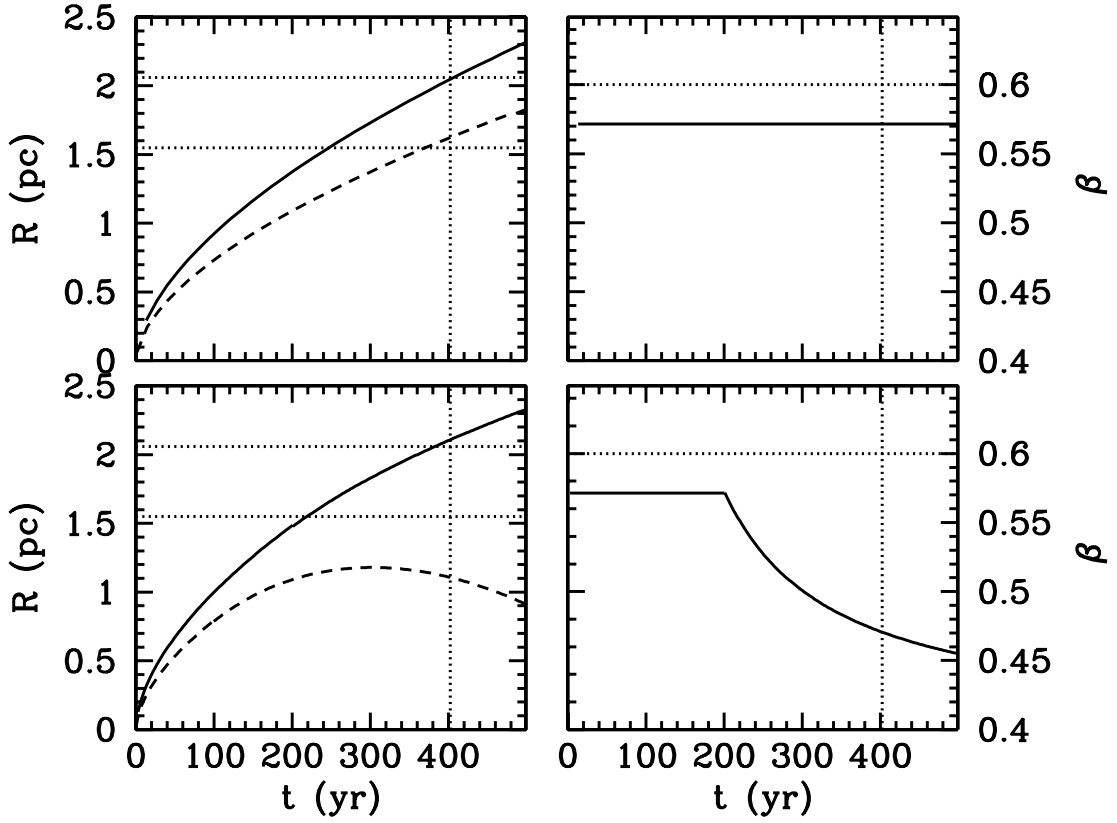

FIG. 9.—Evolution of shock radii (*left*) and expansion parameters of the forward shock (*right*) according to the $n = 7$ model of Truelove & McKee (1999) for two different sets of kinetic energies and circumstellar densities. The values were adapted such that the forward shock matches 2.06 pc (indicated by the upper dotted line) at the age of Kepler's SNR (402 yr), valid for a distance of 4 kpc. In the top panels $n_{\rm H} = 1$ cm^{-3}, resulting in a kinetic energy of $E_0 = 2 \times 10^{50}$ erg. In the bottom panels $E_0 = 10^{51}$ erg, in which case $n_{\rm H} = 12$ cm^{-3}. In this case both the position of the reverse shock (the lower dotted line in the left panels) and the expansion parameter do not match the measurements. [*See the electronic edition of the Journal for a color version of this figure.*]

reinforces the idea of a dense shell that has recently been encountered by the blast wave.

As noted by Reynolds et al. (2007) the presence of nitrogen-rich material from the progenitor system is difficult, but not impossible, to reconcile with SN 1604 being a Type Ia supernova. A possibility is, for example, that the supernova belonged to the short-lived Type Ia channel (Mannucci et al. 2006), in which the white dwarf progenitor and its companion star were relatively massive stars. However, for the remnant of SN 1604 the complication remains that the progenitor, or its companion, must have deposited a substantial amount of mass at a large distance.

The amount of material must have been substantial in order for the shock to have decelerated so much that the expansion parameter is even lower than expected for the Sedov-Taylor phase. If we assume that the material encountered in the northwest was a shell, covering a fraction of about $f = 0.25$, one can estimate the mass in the shell by requiring that the mass in the shell must be more than the swept-up interstellar medium in other parts of the remnant, which have $n_{\rm H} \approx 1$ cm^{-3}. This corresponds to a mass of $M_{\rm swept} = 1(f/0.25) n_{\rm H} d_4^3\, M_\odot$. It therefore seems reasonable to assume that the mass encountered in the northwest is also about 1 $M_\odot$.

This material must have been lost either from the progenitor of the supernova or from its companion star. This suggests a strongly nonconservative binary evolution scenario: too much mass in the shell means less mass available for accretion onto the white dwarf, complicating its evolution toward a Type Ia supernova. Another problem may be how to eject this material to a distance of $\sim$2 pc from the progenitor. Perhaps the shell is caused by nova explosions on the progenitor?

The remnant of SN 1604 remains, therefore, a puzzling but intriguing object. Due to its unusual properties it may in the future reveal new aspects of Type Ia supernovae. Future studies of the SNR may provide some answers, but a high priority would be to identify light echoes of SN 1604 and obtain their optical spectra. This has been done very recently for the SNRs Cas A (Krause et al. 2008), which appears to have been a Type IIb supernova, and SNR 0509−67.5, an energetic Type Ia supernova in the Large Magellanic Cloud (Rest et al. 2008).

5. SUMMARY

The expansion of Kepler's SNR (SN 1604) was measured using archival *Chandra* data. The expansion in all parts of the remnant is inconsistent with free expansion with the expansion measurement of $\beta \approx 0.9$, that was previously reported (Hughes 1999).

The X-ray measurements reported here, and previous radio and optical expansion measurements, show that the remnant expands more slowly in the bright northwestern part, $\beta \approx 0.3$–0.4, than in the rest of the supernova remnant, where $\beta \approx 0.6$. The fastest expansion is found for the X-ray synchrotron filament in the eastern part of the remnant, $\beta \approx 0.7$.

The remnant seems not yet to have entered the Sedov-Taylor phase of its evolution: Apart from the northwestern region the expansion parameters are consistent with the early expansion phase as detailed in the models by Chevalier (1982), Truelove & McKee (1999), and Dwarkadas & Chevalier (1998). For the northwestern part of the remnant a different scenario is needed, since its expansion parameter is even smaller than for a Sedov-Taylor evolution model.

The kinematics of Kepler's SNR, in particular the more undisturbed southwestern region, is only consistent with current hydrodynamical models of Type Ia SNRs if its distance is considerably larger than the 4 kpc obtained by Sankrit et al. (2005). Recently, Aharonian et al. (2008) suggested that $d > 6$ kpc, based on the nondetection of Kepler by the H.E.S.S. TeV γ-ray telescope. Both in the present paper and in Aharonian et al. (2008) the conclusion regarding a large distance is based on the assumption that Kepler was indeed a Type Ia SNR with an explosion energy $\gtrsim 10^{51}$ erg. The X-ray synchrotron filament seems to move with a shock speed of $4200 d_4$ km s^{-1}, consistent with theory (Aharonian & Atoyan 1999) and other observations (Helder & Vink 2008) that indicate that only shocks with $v_s \gtrsim 2000$ km s^{-1} emit X-ray synchrotron radiation.

This work is supported by a Vidi grant from the Netherlands Organisation for Scientific Research (NWO). I would like to thank Eveline Helder, Klara Schure, Frank Verbunt, and Daria Kosenko for discussions and helpful comments on the manuscript. In addition, I thank Eveline Helder for providing me with Figure 8.

REFERENCES

Aharonian, F., et al. 2008, A&A, 488, 219
Aharonian, F. A., & Atoyan, A. M. 1999, A&A, 351, 330
Baade, W. 1943, ApJ, 97, 119
Bamba, A., et al. 2005, ApJ, 621, 793
Bandiera, R. 1987, ApJ, 319, 885
Bell, A. R. 2004, MNRAS, 353, 550
Bell, A. R., & Lucek, S. G. 2001, MNRAS, 321, 433
Blair, W. P. 2005, in ASP Conf. Ser. 342, 1604–2004: Supernovae as Cosmological Lighthouses, ed. M. Turatto et al. (San Francisco: ASP), 416
Blair, W. P., Long, K. S., & Vancura, O. 1991, ApJ, 366, 484
Cash, W. 1979, ApJ, 228, 939
Cassam-Chenaï, G., et al. 2004, A&A, 414, 545
Chevalier, R. A. 1982, ApJ, 258, 790
Delaney, T., & Rudnick, L. 2003, ApJ, 589, 818
Dickel, J. R., Sault, R., Arendt, R. G., Korista, K. T., & Matsui, Y. 1988, ApJ, 330, 254
Dwarkadas, V. V., & Chevalier, R. A. 1998, ApJ, 497, 807
Fesen, R. A., Becker, R. H., Blair, W. P., & Long, K. S. 1989, ApJ, 338, L13
Helder, E. A., & Vink, J. 2008, ApJ, 686, 1094
Hughes, J. P. 1999, ApJ, 527, 298
———. 2000, ApJ, 545, L53
Kinugasa, K., & Tsunemi, H. 1999, PASJ, 51, 239
Koralesky, B., Rudnick, L., Gotthelf, E. V., & Keohane, J. W. 1998, ApJ, 505, L27
Krause, O., Birkmann, S. M., Usuda, T., Hattori, T., Goto, M., Rieke, G. H., & Misselt, K. A. 2008, Science, 320, 1195
Malkov, M. A., & Drury, L. 2001, Rep. Prog. Phys., 64, 429
Mannucci, F., Della Valle, M., & Panagia, N. 2006, MNRAS, 370, 773
Mazzali, P. A., Röpke, F. K., Benetti, S., & Hillebrandt, W. 2007, Science, 315, 825
Rest, A., et al. 2008, ApJ, 680, 1137
Reynolds, S. P., Borkowski, K. J., Hwang, U., Hughes, J. P., Badenes, C., Laming, J. M., & Blondin, J. M. 2007, ApJ, 668, L135
Reynoso, E. M., & Goss, W. M. 1999, AJ, 118, 926
Sankrit, R., Blair, W. P., Delaney, T., Rudnick, L., Harrus, I. M., & Ennis, J. A. 2005, Adv. Space Res., 35, 1027
Stage, M. D., Allen, G. E., Houck, J. C., & Davis, J. E. 2006, Nature Phys., 2, 614
Stephenson, F. R., & Green, D. A. 2002, Historical Supernovae and Their Remnants (Oxford: Clarendon)
Truelove, J. K., & McKee, C. F. 1999, ApJS, 120, 299
Vink, J. 2004, Adv. Space Res., 33, 356
———. 2006, in The X-Ray Universe 2005, Vol. 1, ed. A. Wilson (ESA SP-604; Noordwijk: ESA), 319
Vink, J., Bleeker, J., van der Heyden, K., Bykov, A., Bamba, A., & Yamazaki, R. 2006, ApJ, 648, L33
Vink, J., Bloemen, H., Kaastra, J. S., & Bleeker, J. A. M. 1998, A&A, 339, 201
Vink, J., & Laming, J. M. 2003, ApJ, 584, 758
Völk, H. J., Berezhko, E. G., & Ksenofontov, L. T. 2005, A&A, 433, 229
Warren, J. S., et al. 2005, ApJ, 634, 376
Woosley, S. E., Kasen, D., Blinnikov, S., & Sorokina, E. 2007, ApJ, 662, 487